two differential equations of the second approximation. They are of the forms

$$\zeta'''_{1a}+2\eta\zeta''_{1a}-12\zeta'_{1a}=4(-1+\zeta_0{}^2-\zeta_0\zeta''_0) \tag{10}$$

$$\zeta'''_{1b}+2\eta\zeta''_{1b}-12\zeta'_{1b}=4\zeta''_0\zeta_0 \tag{11}$$

with the boundary conditions $\eta=0$, $\zeta_{1a}=\zeta'_{1a}=\zeta_{1b}=0$; $\eta=\infty$, $\zeta'_{1a}=\zeta'_{1b}=0$. ζ_{1a} is identical with the second approximation equation of two dimensional case which has also been solved by Blasius.[1] ζ_{1b} has been calculated by computer. Its shape is shown in Fig. 1. The initial slope of ζ'_{1b} is $\zeta''_{1b}(0)=0.0904608$.

Inserting Eq. (7) and Eq. (8) into Eq. (5) we obtain five differential equations of the third approximation

$$\begin{aligned}
&\zeta'''_{2a}+2\eta\zeta''_{2a}-20\zeta'_{2a}=-4(\zeta_{1a}\zeta''_0-\zeta'_{1a}\zeta'_0)\\
&\zeta'''_{2b}+2\eta\zeta''_{2b}-20\zeta'_{2b}=-4(\zeta_{1a}\zeta''_0+2\zeta_{1b}\zeta''_0-3\zeta'_{1b}\zeta'_0\\
&\qquad\qquad+\zeta''_{1b}\zeta_0+\zeta''_{1a}\zeta_0)\\
&\zeta'''_{2c}+2\eta\zeta''_{2c}-20\zeta'_{2c}=-4(\zeta_{1b}\zeta''_0-\zeta'_{1b}\zeta'_0)\\
&\zeta'''_{2c}+2\eta\zeta''_{2d}-20\zeta'_{2d}=-4(\zeta_{1a}\zeta''_0-2\zeta'_{1a}\zeta'_0+\zeta''_{1a}\zeta_0)\\
&\zeta'''_{2e}+2\eta\zeta''_{2e}-20\zeta_{2e}=-4(\zeta'_{1b}\zeta'_0+\zeta''_{1a}\zeta_0)
\end{aligned} \tag{12}$$

with the boundary conditions $\eta=0$, $\zeta_{2a}=\zeta_{2b}=\zeta_{2c}=\zeta_{2d}=\zeta_{2e}=\zeta'_{2a}=\zeta'_{2b}=\zeta'_{2c}=\zeta'_{2d}=\zeta'_{2e}=0$; $\eta=\infty$, $\zeta'_{2a}=\zeta'_{2b}=\zeta'_{2c}=\zeta'_{2d}=\zeta'_{2e}=0$.

Equation (12) has been calculated by computer. The function ζ'_{2a}, ζ'_{2b}, ζ'_{2c}, ζ'_{2d}, and ζ'_{2e} are shown in Fig. 2. The initial slopes of the five functions are

$$\begin{aligned}
\zeta''_{2a}(0)&=-0.0218086\\
\zeta''_{2b}(0)&=-0.00333173\\
\zeta''_{2c}(0)&=-0.00589340\\
\zeta''_{2d}(0)&=-0.0636076\\
\zeta''_{2e}(0)&=-0.0101829
\end{aligned}$$

The velocity gradient can be evaluated from Eq. (7)

$$\frac{\partial u}{\partial y}=\frac{wt}{2(vt)^{1/2}}\left[\zeta''_0+t^2\frac{dw}{dx}\zeta''_{1a}+\frac{wt^2}{r}\frac{dr}{dx}\zeta''_{1b}+\right.$$

$$wt^4\frac{d^2w}{dx^2}\zeta''_{2a}+\frac{wt^4}{r}\frac{dr}{dx}\frac{dw}{dx}\zeta''_{2b}+w^2t^4\frac{1}{r}\frac{dw}{dx^2}\zeta''_{2c}+$$

$$\left.t^4\left(\frac{dw}{dx}\right)^2\zeta''_{2d}+w^2t^4\frac{1}{r^2}\left(\frac{dr}{dx}\right)^2\zeta''_{2e}\right] \tag{13}$$

For a sphere with radius R the potential velocity is

$$U(x,t)=tw(x)=t(3/2)a\sin(x/R)$$

and $r=R\sin(x/R)$. It is known that separation occurs at a downstream stagnation point. Substituting the above relations and the initial slopes of the various functions in Eq. (13), we obtain separation time t_s from the following relation

$$2.256758-1.05212(3/2)(a/R)t_s^2-$$

$$0.05675643[(3/2)(a/R)t_s^2]^2=0$$

Thus $t_s=1.1374(R/w)^{1/2}$. If only the second approximation is considered the separation time is $t_s=1.1950(R/a)^{1/2}$ which is about 5% larger than the value given by the third approximation.

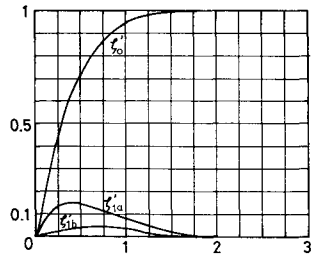

Fig. 1 The functions ζ'''_0, ζ'''_{1a} and ζ'''_{1b} for the velocity distribution in the nonsteady boundary layer

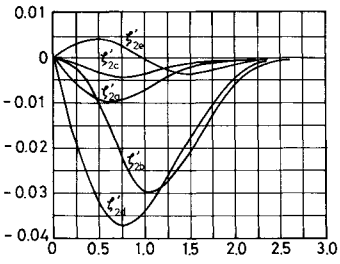

Fig. 2 The functions ζ'''_{2a}, ζ'''_{2b}, ζ'''_{2c}, ζ'''_{2d} and ζ'''_{2e} for the velocity distribution in the nonsteady boundary layer.

References

[1] Schlichting, H., *Boundary Layer Theory*, 6th ed., McGraw-Hill, New York, 1968, p. 406.

Leading-Edge Rotating Cylinder for Boundary-Layer Control on Lifting Surfaces

W.S. Johnson,* J.S. Tennant,* and R.E. Stamps†
University of Tennessee, Knoxville, Tenn.

Nomenclature

C_p = surface pressure coefficient
G = gap between fixed and moving surfaces (in.)
R = cylinder radius (in.)
Re = Reynolds number based on U_∞ and R
U_∞ = freestream velocity
U_c = cylinder surface velocity
X = dimensionless distance from leading edge of body

Introduction

THE use of boundary-layer control to increase the maximum lift on an airfoil has been well documented by many investigators and methods such as suction, blowing, vortex generators, turbulence promotion, etc., have found practical application in many situations. The use of a moving wall for boundary-layer control has been under investigation for many years, for example Refs. 1–3. However, until recently no serious attempts have been made to utilize the moving wall concept.

Received October 29, 1974.
Index categories: Boundary Layers and Convective Heat Transfer—Turbulent, Marine Hydrodynamics, Vessel and Control Surface.

* Associate Professor. Member AIAA.
† Research Assistant.

In 1961, Alvarez-Calderon and Arnold[4] employed a rotating cylinder to control the boundary layer over a deflected flap and this configuration is currently being tested for use with STOL type aircraft. Tennant[5] successfully applied the moving wall concept to air flow through a diffuser and reported a completely detailed numerical calculation technique to predict diffuser behavior. Steele[6] investigated the use of a rotating cylinder as the leading edge of a ship's rudder and reported remarkable improvements in maneuverability, both from full-scale tests on a 200 ton cargo ship and on a radio-controlled model ship. No detailed data has been reported however. This note describes detailed wind tunnel studies of the boundary-layer control attained on a symmetrical afterbody by utilizing a rotating cylinder at its leading edge.

Approach

A model 13.5 in. long having a 3 in. diam cylinder and constant taper as shown in Fig. 1 was tested in a subsonic wind tunnel having an open circuit with a 20×28 in. test section. The model was mounted between the upper and lower walls of the wind tunnel with both cylinder and afterbody extending through the tunnel walls to approximate a two-dimensional flow condition. Static pressure taps were located chordwise near the center of the body and the entire suction side of the body as well as adjacent tunnel walls was instrumented with tufts to indicate the existence of flow separation.

Measurements were made at various angles of attack up to 15° and at speeds from 30 to 60 mph. At each condition, the cylinder speed was increased until separation was eliminated on the body as evidenced by tuft behavior. Once the separation was eliminated, the static pressure distribution over the body was recorded.

In an effort to determine the effect of the gap between the rotating and fixed surfaces on the boundary layer control actually obtained, tests were run at various gaps from 0.010 to 0.035 in. at an angle of attack of 7.5°.

A prediction of the pressure distribution on the model was obtained by the procedure of Smith[7] which solves the Newman problem. The calculation model utilized two bodies in an infinite cascade with a plane of symmetry in order to simulate the effects of the wind tunnel side walls. Since the model had a sharp trailing edge, the Kutta condition was imposed on the solution.

Results and Discussion

The ratio of cylinder surface velocity to freestream air velocity required to unstall the flow on the suction side of the model at various angles of attack is given in Fig. 2 for a gap of 0.020 in. The required speed ratio is seen to increase with angle of attack as expected due to increasing adverse pressure gradient and this variation is almost linear.

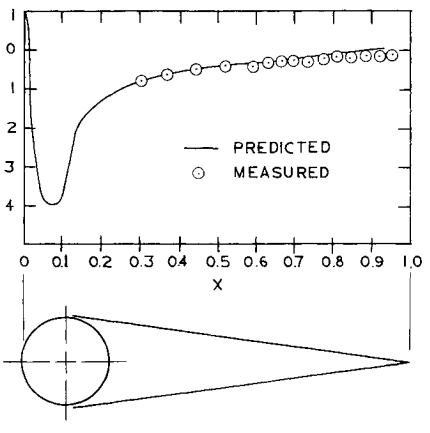

Fig. 1 Surface pressure coefficient (suction side) for a 5° angle of attack.

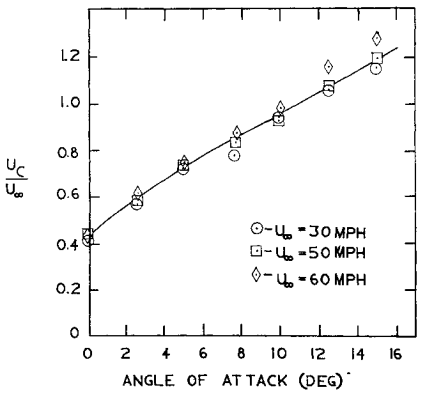

Fig. 2 Velocity ratio required to prevent separation vs angle of attack.

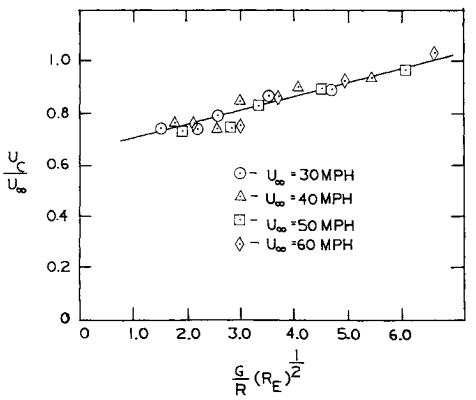

Fig. 3 Velocity ratio required to prevent separation vs gap parameter (7.5° angle of attack).

An increase in the required speed ratio was found for higher tunnel speeds and it appears that this results from decreased boundary-layer thickness at the higher freestream speeds which allows a larger fraction of the boundary layer to pass through the gap rather than flow along the body.

Figure 3 shows the effect of the gap between fixed and moving surfaces on the speed ratio to eliminate separation at an angle of attack of 7.5°. By introducing the parameter $G/R(Re)^{1/2}$ the plot becomes almost linear and the additional dependance of tunnel speed is eliminated. This nondimensional parameter is based on the assumption that the boundary layer is laminar at the gap and its thickness is inversely proportional to $(Re)^{1/2}$ as in the case of flow about a fixed cylinder.

Even though the main flow on the body could be unstalled by operation of the cylinder, separation to some degree was always present. Even at an angle of attack of 0° separation existed in a very small region at the intersection of the model with the tunnel walls. This was due to the boundary layer which had accumulated on the walls of the wind tunnel prior to reaching the model and the adverse pressure gradient existing on the fixed portion of the body at zero angle of attack. The low-energy portion of the layer could not be energized sufficiently by the cylinder to prevent separation over the body. As the angle of attack was increased, the region of separation also increased in size. Separation was initiated at the body-tunnel wall junction just downstream of the cylinder and spread on both the model and tunnel walls toward the downstream end. At the highest angle of attack (15°) this separated region had spread such that the entire trailing edge was separated leaving a triangular region of unseparated flow in the center region of the model.

The comparison of measured and predicted pressure coefficients on the suction side of the model indicates the degree to

which the measured data represents actual two-dimensional flow. Figure 1 shows this comparison for an angle of attack of 5°, and indicates quite good agreement. This agreement was improved at low angles of attack and was poorer at the higher angles when separation altered the two-dimensional nature of the flow.

Conclusions

A rotating cylinder at the leading edge of a lifting body can effectively control boundary-layer separation as evidenced by experimental results. The upper limit on the angle of attack without separation was a result of boundary-layer accumulation on the wind-tunnel walls and consequently does not represent a limitation in applications. Also, the two-dimensional configuration as tested presents higher adverse pressure gradients and thus a more difficult boundary-layer control application than a lifting body having finite span. The gap between the cylinder and the fixed afterbody has been shown to be a significant parameter. This gap should be maintained at its minimum practical value in order to minimize the cylinder speed required for effective boundary-layer control.

References

[1] Thwaites, B., ed., *Incompressible Aerodynamics,* Clarendon Press, Oxford, 1960. p. 215.

[2] Goldstein, S., ed., *Modern Developments in Fluid Dynamics,* Clarendon Press, Oxford, 1938. p. 78.

[3] Farve, M.A., "Un nouveau procede hypersustenateur: l'aile a' parol d' extrados mobile," *Mechanique Expermentale Des Fluids,* Comtes Rendus, 1934. p. 634.

[4] Alvarez-Calderon, A., and Arnold, F.A., "A Study of the Aerodynamic Characteristics of a High-Lift Device Based on a Rotating Cylinder Flap," Tech. Rept. RCF-1, Sept. 1961, Stanford University, Stanford, Calif.

[5] Tennant, J.S., "A Subsonic Diffuser With Moving Walls for Boundary Layer Control," *AIAA Journal,* Vol. 11, Feb. 1973, p. 240.

[6] Steele, B.N. and Harding, M.H., "The Application of Rotating Cylinders to Ship Maneuvering," National Physical Laboratory (Britain) Ship Rept. 148, Dec. 1970.

[7] Smith, A.M.O., "Exact Solution of the Newman Problem. Calculation of Non Circulatory Plane and Axially Symmetric Flows About or Within Arbitrary Boundaries," Rept. ES 26988, April 1958, Douglas Aircraft Co., Long Beach, Calif.

Calculations of the Turbulent Wake Behind Slender Self-Propelled Bodies with a Kinetic Energy Method

Roy C. Swanson Jr.* and Joseph A. Schetz†
Virginia Polytechnic Institute and State University
Blacksburg, Va.

Nomenclature

a_1 = factor in Eq. (1)
D = diameter
k = turbulent kinetic energy
U = axial velocity
U_E = freestream velocity
U_C = centerline velocity
X = axial coordinate
ρ = density
τ = shear
$-\overline{u'v'}$ = Reynolds stress

Received January 13, 1975. This work was supported by the Advanced Research Projects Agency. Technical monitoring was by the Office of Naval Research.

Index categories: Jets, Wakes, and Viscid-Invisoid Flow Interaction; Viscous Nonboundary-Layer Flows; Marine Hydrodynamics, Vessel and Control Surface.

*Graduate Research Assistant, Aerospace and Ocean Engineering Department, now at Naval Surface Weapons Center.

†Professor and Department Chairman, Aerospace and Ocean Engineering Department. Associate Fellow AIAA.

Introduction

THERE has been a relative scarcity of experimental and theoretical information on the behavior of turbulent wakes behind self-propelled bodies. An extensive experimental program concerning slender bodies at high Reynold's number ($Re_D \approx 600{,}000$) has recently been completed and reported in Refs. 1-3. There were three models studied, all with the same forebody shape. The first (Model#1) was simply a drag-body with a sharp stern. Model #2 was self-propelled by means of axial injection through a peripheral slot, and Model #3 was driven by a propeller.

To complement these experiments, calculations of wake development were made using the kinetic energy formulation of Harsha,[4] and this Note serves to report the results of that undertaking. Some modifications to the basic approach were found necessary[4] to handle the momentumless cases. A key relationship in the formulation is that between shear τ and the local kinetic energy k, and for normal free shear flows the following has been employed

$$\tau = a_1 \rho k \tag{1}$$

where ρ is the density and $a_1 = 0.3$. Although a_1 can be taken as a constant value of 0.3 over most of the wake flow, it is not a constant in the vicinity of the centerline since the shear stress vanishes at that point for axisymmetric flows; in this program we have used[4]

$$a_1 = 0.3 \frac{\partial U/\partial R}{|\partial U/\partial R|_{\max}} \tag{2}$$

for normal shear flows, i.e., Model #1. This relation was applied from the centerline to the point $\partial U/\partial R = (\partial U/\partial R)_{\max}$. Beyond that point

$$a_1 = 0.3 \frac{\partial U/\partial R}{|\partial U/\partial R|} \tag{3}$$

which yields the proper sign. To avoid an excessive shear stress value in the outer region of the flow for momentumless cases, the program was modified[4] to include the following formulation:

$$a_1 = 0.3 \frac{\partial U/\partial R}{|\partial U/\partial R|_{\max}} \quad \partial U/\partial R > 0$$
$$a_1 = 0.3 \frac{\partial U/\partial R}{|(\partial U/\partial R)_{\min}|} \quad \partial U/\partial R < 0 \tag{4}$$

Complete information on modeling of the other terms in the turbulent kinetic energy equation, i.e., dissipation and diffusion terms, is provided in Ref. 5. Note, all parameters involved in modeling were taken as the normal values, as dictated by previous experiments, generally not momentumless. This was necessary since our recent experimental effort did not penetrate the regime of statistical flow characteristics, i.e., turbulence length scale, autocorrelation functions, and energy spectrum.

Results

Since the formulation is parabolic, the principal information required to undertake a calculation is in the form